Periodica Polytechnica
Civil Engineering

61 (4), pp. 939–950, 2017
https://doi.org/10.3311/PPci.10548

RESEARCH ARTICLE

Seismic Failure Probability and Vulnerability Assessment of Steel-Concrete Composite Structures

Masoud Ahmadi[1*], Hosein Naderpour[1], Ali Kheyroddin[1], Amir H. Gandomi[2]

Received 27 January 2017; Revised 02 April 2017; Accepted 18 April 2017

Abstract

Building collapse in earthquakes caused huge losses, both in human and economic terms. To assess the risk posed by using the composite members, this paper investigates seismic failure probability and vulnerability assessment of steel-concrete composite structures constituted by rectangular concrete filled steel tube (RCFT) columns and steel beams. To enable numerical simulation of RCFT-structure, the details of components modeling are developed using OpenSEES finite element analysis package and the validation of proposed procedure is investigated through comparisons with available experimental results. The seismic fragility and vulnerability curves of RCFT-structures are created through nonlinear dynamic analysis using an appropriate suite of ground motions for seismic loss assessment. These curves developed for three-, six- and nine-story prototypes of RCFT-structure. Fragility curves are an appropriate tool for representing the seismic failure probabilities and vulnerability curves demonstrate a probability of exceeding loss to a measure of ground motion intensity.

Keywords

steel-concrete structures, failure probability, performance-based seismic design, fragility curve, seismic vulnerability

[1] Faculty of Civil Engineering,
Semnan University,
Semnan, Iran
[2] BEACON Center for the Study of Evolution in Action,
1450 BPS, Michigan State University,
East Lansing, MI 48824, USA
*Corresponding author email: masoud.ahmadi@semnan.ac.ir

1 Introduction

Steel-concrete composite structural system is progressively becoming popular in construction of buildings because of their excellent performance [1, 2]. Concrete-filled steel tube (CFT) columns in combination with steel beams (Fig. 1) is one of the most successful lateral load resisting systems in the construction industry [3, 4]. A CFT column, when designed appropriately, has superior strength and ductility in comparison with hollow steel tube. The CFT column is also more economical than conventional reinforced concrete column because of optimal location of steel at the periphery of the cross section, rapid construction, and role of steel tube as stay-in-place formwork. In CFT columns, concrete delays local buckling of the steel tube and heightens global buckling resistance of the member. Furthermore, peripheral steel tube adds lateral confinement to the concrete, which induces an increase in compressive strength and ductility of concrete.

In recent decades, considerable investigations have been carried out to characterize the seismic behavior evaluation of concrete filled steel tube system. These studies were focused on components (column and connection) and CFT-frame structures. A wide range of prior researches was conducted on components of CFT-systems. So far, research on CFT-moment resisting frame (MRF) structures, which consist of CFT columns and steel beams, has been limited [5–9]. In recent years, notable studies have been dedicated to the attempt to perceive the seismic performance of composite buildings [10–12].

Sakino et al. [13] investigated the centrally loaded behavior and proposed methods to determine the axial capacity of the CFT columns. Varma et al. [14] performed a series of experimental tests on CFT beam-columns under cyclic loading. They compared their results with provisions of ACI (1999) and AIJ (1987) codes. Tort and Hajjar [15] proposed a finite element method to characterize the behavior of rectangular CFT members subjected to various types of loads.

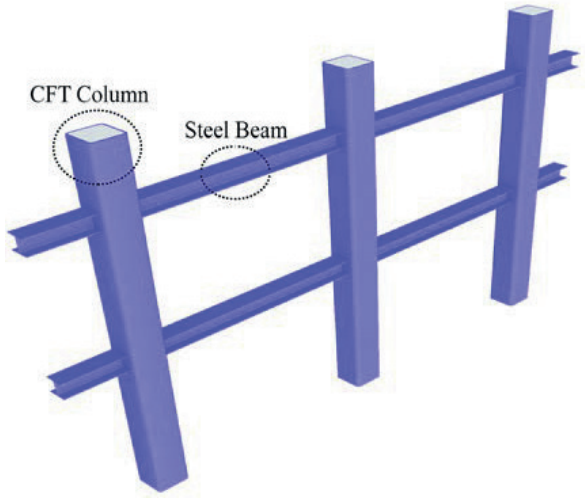

Fig. 1 Schematic illustration of the CFT-frame structure.

Perea et al. [16, 17] and Lai et al. [18] reported experimental and analytical data on the axial and interaction behavior of slender concrete-filled tubes. Skalomenos et al. [19] presented three hysteretic models to investigate the nonlinear response of square CFT column. Ahmadi et al. [20, 21] and Kheyroddin et al. [22] focused on the axial strength of CFT stub columns. They suggested an empirical equation and artificial neural network method for determining the axial capacity of CFT member using a large number of experimental specimens. Lai and Varma [23] focused on effective stress-strain relationships of CFT columns. Xiang et al. [24] investigated the effect of the replacement ratio on the axial behavior of square recycled aggregate CFT column. Ricles et al. [25] and Wang et al. [26] conducted experimental tests on exterior beam to column connections to investigate the inelastic performance of connections in MRF systems. Ataei et al. [27] described the experimental results of full-scale connection of a beam to a composite column. They investigated the failure modes and rotation response of the suggested detail, and developed equations to determine the flexural capacity, initial stiffness, and rotational capacity. A joint element was developed by Kang et al. [28] based on the force-transfer and damage mechanisms.

Kawaguchi et al. [5] carried out an experimental study on one-bay portal frames under constant axial load and cyclic lateral loading. The results show that all frames have appropriate hysteresis performance. Herrera et al. [6] carried out pseudo-dynamic test on a four-story composite MRF which consist of steel-concrete columns and steel beams. Results denoted that CFT-Fame has desirable structural performance under various seismic loading levels. Tort and Hajjar [7], and Denavit and Hajjar [8, 9], developed three-dimensional distributed plasticity finite element formulations for modeling inelastic behavior of composite frame under seismic loading. The exactness of the proposed formulations was checked with a wide range of experimental tests. The seismic analysis and damage quantification of planar CFT-frame constitute by I steel beams, and CFT columns were investigated by Skalomenos et al. [10] and Kamaris et al. [11]. Denavit et al. [12] reported a comprehensive parametric study to evaluate the stability of steel-concrete composite frame structure and proposed some changes to the AISC (2010) provisions.

2 Research significance

The main goals of this paper are to assess seismic failure probability and develop vulnerability curves of RCFT-frame structures for using in seismic loss assessment studies and performance-based earthquake engineering (PBEE). The past catastrophic earthquakes reveal that large earthquakes can cause extensive losses of life and economic damages. Fragility curves are an appropriate tool for representing the seismic failure probability of building and are used as a needed input for various type of loss assessment software [29]. Furthermore, vulnerability curve is one of the basic instruments to evaluate structural losses before causing economic and human losses [30]. A seismic vulnerability curve illustrates uncertain loss to a measure of ground motion intensity [31]. Nowadays, there are some gaps in the knowledge of behavior and the design provisions of steel-concrete composite structures [32, 33]. Due to insufficient studies on CFT-frames in this research area, and in order to avoid the extensive losses after earthquake events, fragility and vulnerability curves are developed for three prototypes of RCFT-frame structures.

3 Modeling of the RCFT- structure

In this section, the details of modeling procedure of components of the RCFT-frame structure in the Open System for Earthquake Engineering Simulation (OpenSEES) software [34] are explained. These components include: 1) RCFT column, 2) steel beam, and 3) panel zone and connection.

3.1 RCFT column

The fiber-based model of CFT columns proposed by Tort and Hajjar [7] and Denavit [8], was used as the basis for the CFT column model in this study. The concrete material of the model is based on the modified model proposed by Chang and Mander [35] and Tsai [36]. The monotonic compression response is defined by the Eqs. 1–3.

$$\sigma_c(\varepsilon_c) = f_c^{'} \frac{nx}{D(x)} \tag{1}$$

$$D(x) = \begin{cases} 1 + \left(n - \dfrac{r}{r-1}\right)x + \dfrac{x^r}{r-1} & r \neq 1 \\ 1 + (n - 1 + Lnx)\,x & r = 1 \end{cases} \tag{2}$$

$$r = \begin{cases} f_c^{'}/5.2 - 1.9 & \varepsilon_c < \varepsilon_c^{'} \\ \dfrac{1.7h}{t}\sqrt{F_y/E_s}\,\dfrac{f_c^{'}}{F_y} & \varepsilon_c \geq \varepsilon_c^{'} \end{cases} \tag{3}$$

Where, x, r, and n are the normalized strain, post-peak factor, and normalized modulus, respectively; and f_c', F_y, and E_s are the compressive strength of the plain concrete, the yield stress of the steel tube, and elastic modulus of tube, respectively. The stress-strain backbone curve of the tube is based on a set of hardening and flow rules that act upon the incremental strain proposed by Shen et al. [37]. To take the results of local buckling and biaxial stress into account in the tube, monotonic compressive response of steel tube is modified (Fig. 2).

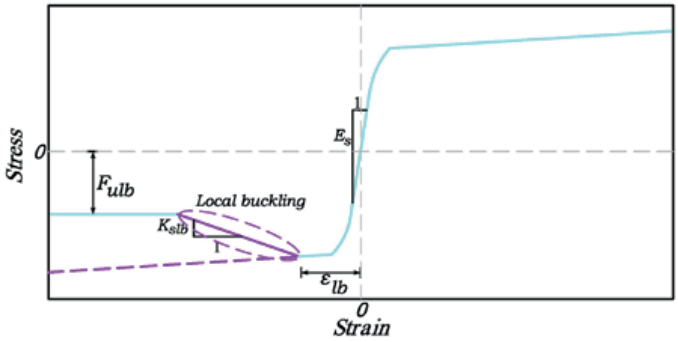

Fig. 2 Modified stress-strain relationship of steel tube considering local buckling effect.

The parameters in modified stress-strain curve are calculated as follows:

$$\varepsilon_{lb} = -3.14\left(\frac{h}{t}\sqrt{F_y/E_s}\right)^{-1.48}\frac{F_y}{E_s} \tag{4}$$

$$F_{ulb} = \left[1+7.31\left(0.08-R\right)\right]F_y \le F_y \tag{5}$$

$$K_{slb} = 3.22\left(0.08-R\right)E_s \tag{6}$$

Where, ε_{lb}, F_{ulb}, and K_{slb} are the strain at local buckling, residual stress, and softening slope, respectively.

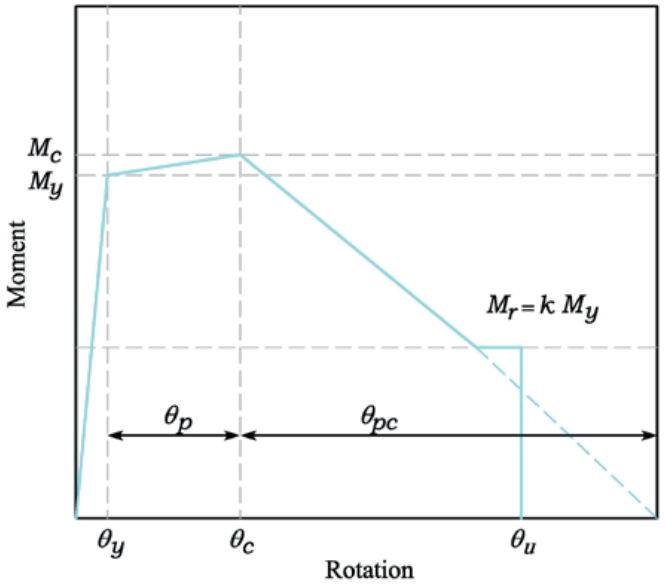

Fig. 3 Monotonic curve of Modified IK deterioration model.

3.2 Steel beam

Ibarra et al. [38] developed hysteretic models that combine the strength and stiffness deterioration. Cyclic deterioration allows tracing deterioration as a function of past loading history. These hysteretic models were modified by Lignos and Krawinkler [39] from a comprehensive database of experimental studies (more than 300 specimens) of wide flange beams (Fig. 3). The key parameters in modified curve are four deformation parameters (yield rotation (θ_y), pre-capping plastic rotation for monotonic loading (θ_p), post-capping plastic rotation (θ_{pc}, ultimate rotation capacity (θ_u)), and three strength parameters (effective yield moment (M_y), capping moment strength (M_c), residual moment (M_r)). Modified Ibarra-Medina-Krawinkler deterioration material model was applied to model the properties of steel beam.

3.3 Panel zone and connection

The model shown in Fig. 4 represents the contribution of the panel zone to nonlinear behavior of CFT-frame structure. The model is consist of two rigid links in order to simulate the rigid extensions of the column and beam; and a rotational spring indicating the relative rotation [40]. The spring should be placed between two nodes in a way that their horizontal and vertical displacement degrees of freedom to be equal. A tri-linear moment-rotation constitutive model determined by the initial stiffness and peak shear strength of panel zone is used in this study. This relationship is resulted from the combination of a bilinear curve for steel, and a tri-linear curve for concrete. The ultimate shear strength and the initial stiffness are determined by superimposing effects of the concrete and steel ingredients.

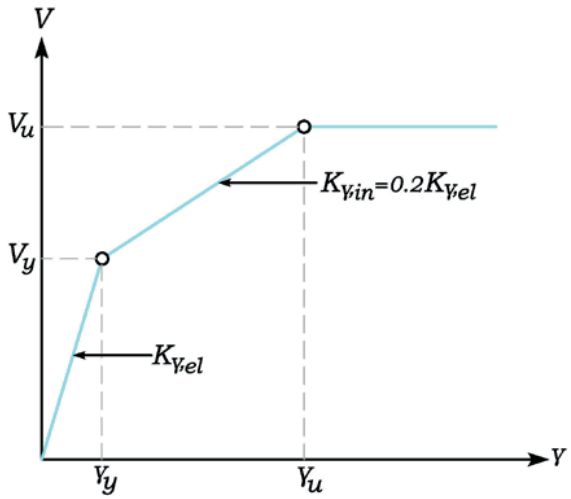

Fig. 4 Tri-linear shear–shear deformation curve for panel zone [40]

The contribution of the steel tube's web to the connection shear strength is calculated as the horizontal shear force that can be resisted by the cross section of the tube's web. For the shear strength of the rectangular tube (V_s) and concrete (V_c), the theoretical mechanism proposed by Krawinkler [41] and Sheet et al. [42] were utilized in this model, which is:

$$V_u = V_s + V_c \Rightarrow \begin{cases} V_s = 0.5774 * (A_{sw} F_y) \\ V_c = 1.99 * \left(A_{cv} f_c^{'0.5} \right) \end{cases} \quad (7)$$

Where, A_{sw} and A_{cv} define the cross section of the tube's web and concrete core, respectively; and F_y and f_c' are the yield stress of the tube and the compressive strength of plain concrete, respectively. The effective shear zone of the rectangular steel tube and concrete are calculated by $2(h–2t_f)t_f$, and $(h–2t_f)(b–2t_f)$, respectively. Where, h is width of tube, b is depth of it, and t_f is its thickness. It is assumed that the yield deformation point corresponds to the yielding of tube. Therefore, the strength and deformation of the web of the steel tube at the yield point are given by Eqs. 8 and 9.

$$V_y = 0.6 V_u \quad (8)$$

$$\gamma_y = \kappa \frac{V_s}{A_{sw} G_w} \quad (9)$$

Where κ = 1.2 for rectangular tube. Based on a research by Muhummud [40], the inelastic stiffness defines 20% of the elastic stiffness ($\kappa_{y,in}$ = 0.2 $\kappa_{y,el}$). The efficiency and accuracy of Eqs. 7 and 9 in modeling CFT-structures were investigated by Skalomenos et al. [10]. The properties assigned to the rotational connection elements are obtained from transforming the load-shear deformation (V – γ) into the moment-rotation (M – θ) for the two elements. The moment of spring is the panel zone shear multiplied by the panel zone depth, which define the beam's depth (d_b), and rotation (θ) of spring is the panel zone deformation γ.

$$M = V * d_b \quad (10)$$

$$\theta = \gamma \quad (11)$$

Furthermore, the connection is modeled using vertical and rotational springs. A vertical spring represents the shear deformation of the connection and a rotational spring is used to model the rotational flexibility of the connection. Both the vertical and rotational springs used in this study have elastic-perfectly plastic behavior model, defined with an initial elastic modulus and a yield point (shown in Fig. 5).

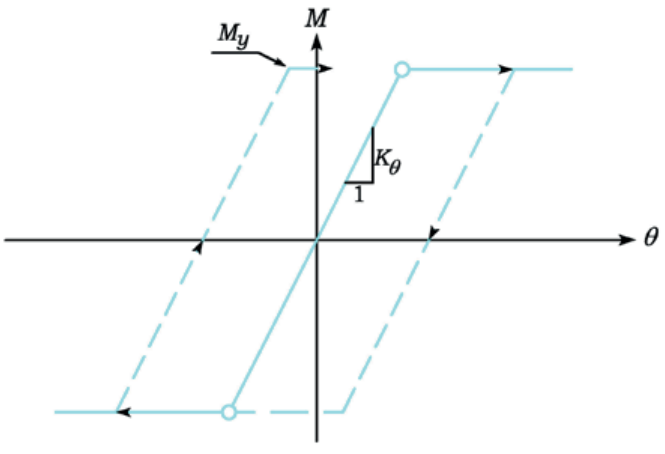

Fig. 5 Connection model spring properties (bilinear model).

4 Verification studies

To verify the precision of the modeling procedure, the cyclic performance of a CFT column and time history response of a CFT-frame will be compared to the experimental results. Varma et al. [14] investigated the response of high strength CFT members subjected to constant axial load and lateral cyclic loading. From Varma's experiments, specimen CBC-48-80-10 is chosen for the verification study. This tested column is 0.75 scale model of a base column of a six-story perimeter MRF. Fig. 6 shows the comparison of the hysteretic response between experimental and numerical result. The results is successfully demonstrated that the proposed modeling procedure can accurately model the hysteretic performance of steel-concrete composite column.

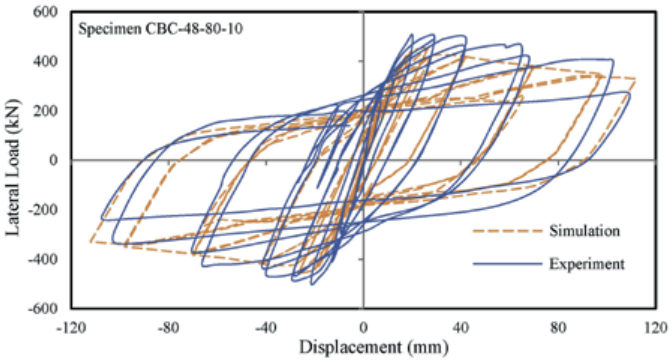

Fig. 6 Comparison of experimental and computational cyclic behavior.

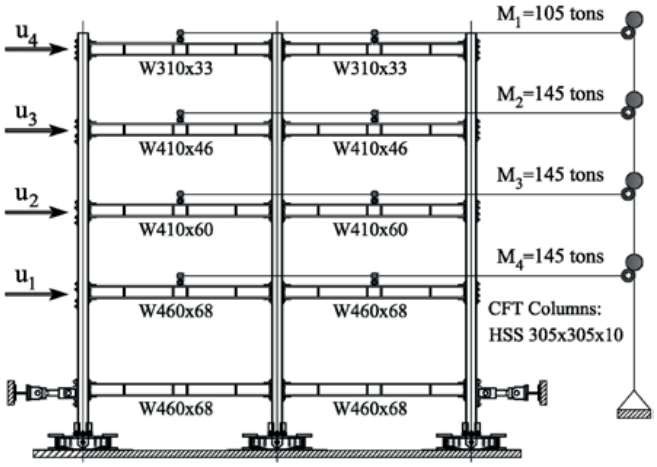

Fig. 7 Test structure elevation [6].

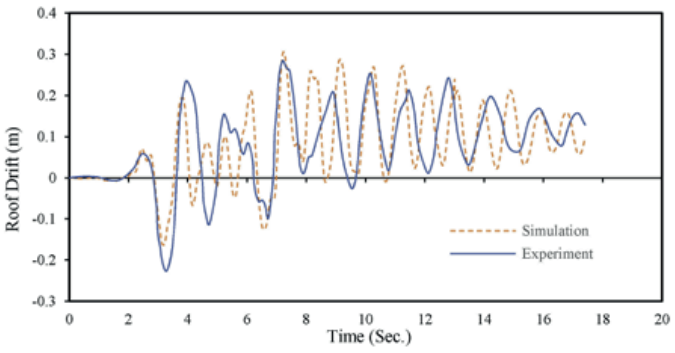

Fig. 8 Comparison of analytical and experimental displacement results of roof floor subjected to the design basis earthquake.

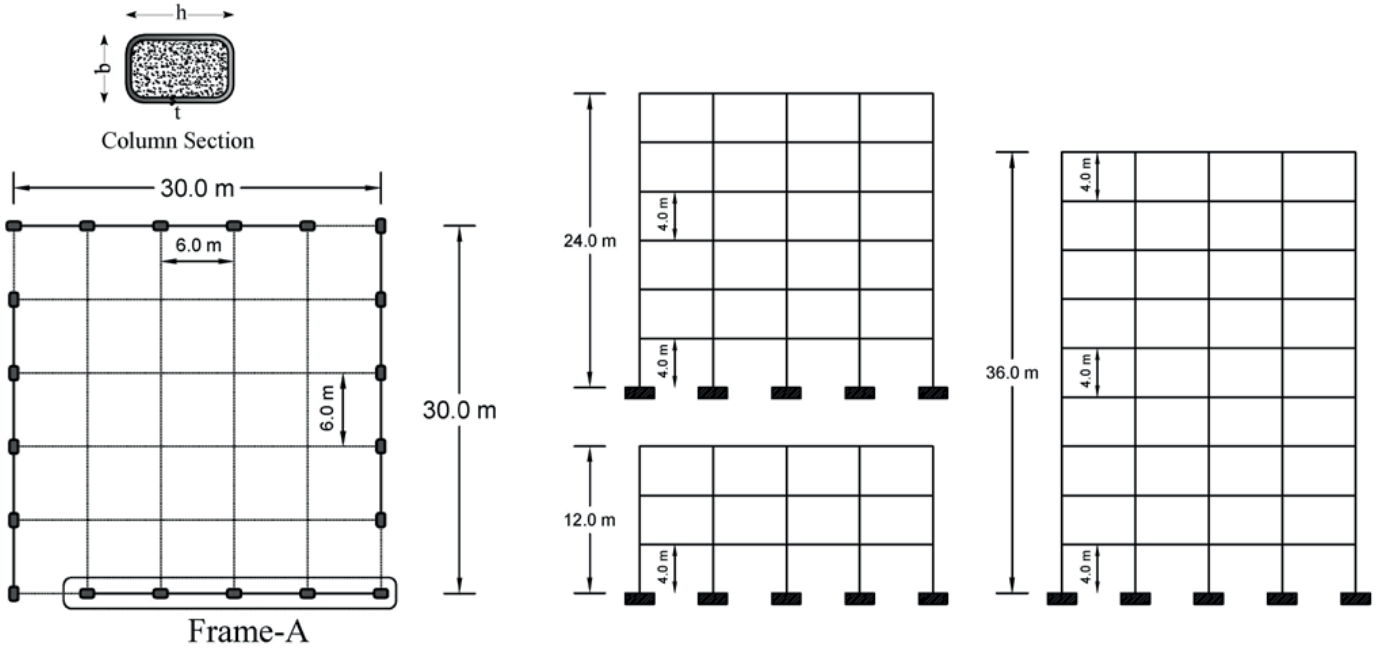

Fig. 9 Prototype floor plan.

Table 1 Characteristics of three types of CFT-MRF structures.

Type	Height (m)	Story	Column			Beam	f_c' (MPa)	$F_{y\text{-}column}$ (MPa)	$F_{y\text{-}beam}$ (MPa)
			h (mm)	b (mm)	t (mm)				
3-Story	12	1–2	500	350	15	W21X62	42	317	345
		3	450	300	15	W18X50	42	317	345
6-Story	24	1–3	500	400	15	W27X114	42	317	345
		4–6	450	350	15	W24X84	42	317	345
9-Story	36	1–3	600	400	20	W30X124	42	317	345
		4–6	500	400	15	W27X114	42	317	345
		7–9	450	300	15	W24X84	42	317	345

Furthermore, the experimental study conducted by Herrera et al. [6] is chosen to evaluate the accuracy of numerical modeling in nonlinear response of CFT-frame subjected to seismic loading condition.

The tested structure is a 0.6 scale model of two bays of one of the perimeter CFT MRFs of the prototype building (Fig. 7). The frame tested under three earthquake levels: 1) the frequently occurring earthquake, 2) the design basis earthquake, and 3) maximum considered earthquake. P-Δ effects due to the lateral displacement of the interior frames are considered by using a lean-on column. The leaning column is pinned at the base, and the lateral movement of it is restricted to each floor by a rigid strut. The lean-on column has cross-section properties corresponding to the sum of the properties of one-half of the gravity columns and one-half of the out of plane properties of the columns of the MRFs which are perpendicular to the direction of loading. The seismic mass is lumped at the node on the leaning column at each floor. Fig. 8 shows the analytical and experimental displacements of roof floor under design basis earthquake. The results denoted that the developed finite element model predicts the seismic response of CFT-MRF structure reasonably well.

5 Building models

To meet the research objectives, three prototype buildings are designed according to the requirements of modern codes [43–45]. They are considered to represent low-rise (three-story), mid-rise (six-story), and high-rise (nine-story) buildings. The floor plan of the prototype buildings (Fig. 9), is 30mx30m area, with five bays of 6m long in each direction. Typical floor to floor height is 4.0m in all buildings. The primary lateral load resisting system consists of RCFT-frame placed on the perimeter of the building. To avoid biaxial bending on the corner columns, only four bays are considered as RCFT-MRFs. The buildings are supposed to be on site in Los Angeles. To investigate the nonlinear behavior of RCFT-structure, Frame-A is selected. The beam to column connections are assumed to be fully rigid in all prototype buildings. These models are implemented in OpenSEES.

Table 2 Selected record from PEER and CESMD

ID No.	Earthquake	Station name	Data	M_w	Component	Database
GM01	Imperial Valley	Calexico Fire Station	1979	6.53	RSN162_IMPVALL.H_H-CXO315.AT2	PEER NGA
GM02	Imperial Valley	El Centro Array #11	1979	6.53	RSN174_IMPVALL.H_H-E11140.AT2	PEER NGA
GM03	Imperial Valley	El Centro Array #3	1979	6.53	RSN178_IMPVALL.H_H-E03230.AT2	PEER NGA
GM04	Imperial Valley	El Centro Array #1	1979	6.53	RSN172_IMPVALL.H_H-E01230.AT2	PEER NGA
GM05	Livermore	Del Valle Dam (Toe)	1980	5.8	RSN212_LIVERMOR_A-DVD246.AT2	PEER NGA
GM06	Livermore	San Ramon - Eastman Kodak	1980	5.8	RSN214_LIVERMOR_A-KOD180.AT2	PEER NGA
GM07	Livermore	San Ramon Fire Station	1980	5.8	RSN215_LIVERMOR_A-SRM070.AT2	PEER NGA
GM08	Irpinia	Bovino	1980	6.9	RSN287_ITALY_A-BOV270.AT2	PEER NGA
GM09	Irpinia	Bisaccia	1980	6.9	RSN286_ITALY_A-BIS000.AT2	PEER NGA
GM10	Irpinia	Brienza	1980	6.9	RSN288_ITALY_A-BRZ000.AT2	PEER NGA
GM11	Coalinga	Pleasant Valley P.P. - yard	1983	6.36	RSN368_COALINGA.H_H-PVY045.AT2	PEER NGA
GM12	Coalinga	Pleasant Valley P.P. - yard	1983	6.36	RSN368_COALINGA.H_H-PVY135.AT2	PEER NGA
GM13	Chalfant Valley	Chalfant - Zack Ranch	1986	6.2	ZACKBRTH.V2	CESMD
GM14	Chalfant Valley	Bishop - South Street	1986	6.2	BISHOPLA.V2	CESMD
GM15	Whittier Narrows	Downey - Co Maint Bldg	1987	5.99	RSN615_WHITTIER.A_A-DWN270.AT2	PEER NGA
GM16	Whittier Narrows	LB - Orange Ave	1987	5.99	RSN645_WHITTIER.A_A-OR2280.AT2	PEER NGA
GM17	Petrolia	Petrolia	1992	7.2	CE89156.V2	CESMD
GM18	Northridge	Castaic - Old Ridge Route	1994	6.69	RSN963_NORTHR_ORR090.AT2	PEER NGA
GM19	Northridge	LA - Temple & Hope	1994	6.69	RSN1005_NORTHR_TEM090.AT2	PEER NGA
GM20	Northridge	Anaverde	1994	6.69	RSN945_NORTHR_ANA180.AT2	PEER NGA
GM21	Northridge	Moorpark - Fire	1994	6.69	RSN1039_NORTHR_MRP090.AT2	PEER NGA
GM22	Chi-Chi	CHY035	1999	7.62	RSN1202_CHICHI_CHY035-E.AT2	PEER NGA

Steel yield strengths are chosen as F_y = 345MPa for steel beam (ASTM A992) and F_y = 317MPa for rectangular HSS shapes (ASTM A500 Gr. B). Data of frames, including building height, column dimensions, and beam type are summarized in Table 1. Gravity loads on the beams of the frames are equal to 1.05 of the dead load plus 0.25 of the live loads of the roof and floors (according to FEMA 2009 [46]). This gravity loading is constant in time history analysis.

6 Selected ground motion records

To carry out nonlinear time history analyses, a suite of 22 ground motions are selected from comprehensive motion databases including the Pacific Earthquake Engineering Next Generation Attenuation [47] Database and the Center for Engineering Strong Motion Data (CESMD) [48]. The site to source distances of selected records are greater than 10km so that they categorized as far-field seismic excitation [46], and the sufficient data about soil conditions of each seismic excitation is available. The moment magnitudes of the records (M_m) range from 5.80 to 7.62. Table 2 shows relevant information about the selected records.

7 Incremental dynamic analysis

Seismic assessment of buildings can be assessed using Incremental Dynamic Analysis (IDA). IDA is a structural analysis method that offers thorough seismic demand and limit-state capacity prediction capability using a series of nonlinear time history analyses (NTHA) under a suite of multiple scaled ground motion records [49]. The procedure of scaling and NTHA is continued to lead the building to inelastic behavior and global dynamic instability. In this study, seismic excitation intensity is measured using the spectral acceleration at the first mode period ($S_a(T_1)$) of the building. Interstory drift ratio, , as a demand parameter, has been proved to be an effective indicator in representing engineering demand [50, 51]. Fig. 10 shows the IDA results for three-, six- and nine-story prototypes under 22 ground motions. The IDA curve depicts the maximum interstory drift ratio (θ_{max}) when the building is under the enhancing level of seismic excitation intensity. These figures contain necessary information to assess performance levels which are important components of PBEE. There are several classifications of building damage states defined in various assessment codes. The damage state levels could be obtained base on recommendation in HAZUS [52] ATC-13 [53], and ASCE-41 [45]. Considering the explanation of the limit states, damage states are considered as none, slight, moderate, extensive, or complete.

8 Seismic fragility and vulnerability analysis

8.1 Procedure of fragility and vulnerability function

Seismic fragility (SF) curve is an outcome of probabilistic analysis accomplished on the results obtained from the IDA curves. Fragility function represents the conditional probability

when the capacity of structures is less than the seismic demand. SF curve can be stated as a lognormal cumulative distribution function as follows:

$$SF \equiv P\left(D > C|IM = x\right) = 1 - \Phi\left[\frac{\ln\left(\hat{C}/\hat{D}\right)}{\beta_{D|IM}}\right] \quad (12)$$

Where, Φ[.] is the Gaussian distribution function of a standard normal variable; IM defines ground intensity measure; $\hat{C}$ and $\hat{D}$ are the median value of structural capacity and the median value of structural demand, respectively; and $\beta_{D|IM}$ is the parameter representing the aleatoric uncertainty of structural demand. In this study, spectral acceleration at the fundamental period ($S_a(T_1)$) and maximum interstory drift ratio (θ_{max}) are selected as IM and D, respectively.

The relationship between the IM and demand can be stated in the power form using Eq. 13.

$$D = a\left(IM\right)^b \quad (13)$$

Where, a and b are regression coefficients that can be calculated by a linear regression analysis of ln(D) versus ln(IM) got from the results. For three-, six- and nine-story structures, the relationship between the logarithmic form of structural demand and seismic intensity measure are shown in Fig. 11. In order to convert fragility curves to vulnerability function, cumulative probabilities are differentiated to obtain discrete probabilities of each level of damage [30]. In particular, the HAZUS discrete probabilities are given as,

$$\begin{aligned}
P[ds = Complete] &= P[ds \geq Complete] \\
P[ds = Extensive] &= P[ds \geq Extensive] \\
&\quad - P[ds \geq Complete] \\
P[ds = Moderate] &= P[ds \geq Moderate] \\
&\quad - P[ds \geq Extensive] \\
P[ds = Slight] &= P[ds \geq Slight] \\
&\quad - P[ds \geq Moderate] \\
Vulnerability\ (\%) &= \sum_{ds=1}^{n} \{P[ds = DS] * MDF_{ds}\}
\end{aligned} \quad (14)$$

Where, MDFds is the mean damage factor, which is the central value of the damage factor range, and ds is the damage state in a given seismic intensity. The various values of MDF, which indicate specified physical building damage, are presented in Table 3.

Table 3 Damage states and damage factor ranges (HAZUS)

Damage states	None	Slight	Moderate	Extensive	Complete
Damage factor range (%)	0	0–4	4–16	16–84	100
Mean damage factor (%)	0	2	10	50	100

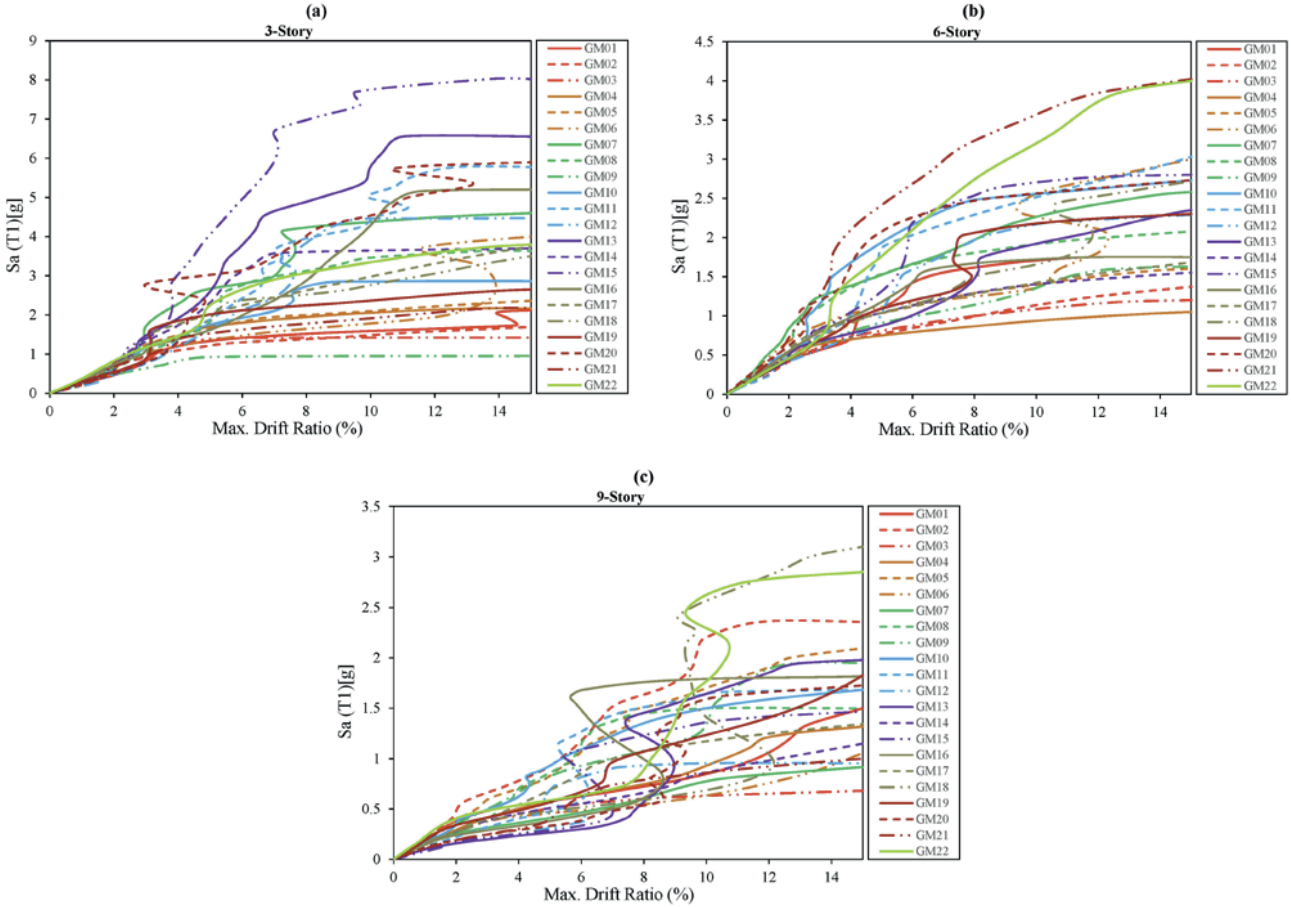

Fig. 10 IDA curves of three prototype buildings: (a) three-story, (b) six-story, and (c) nine-story.

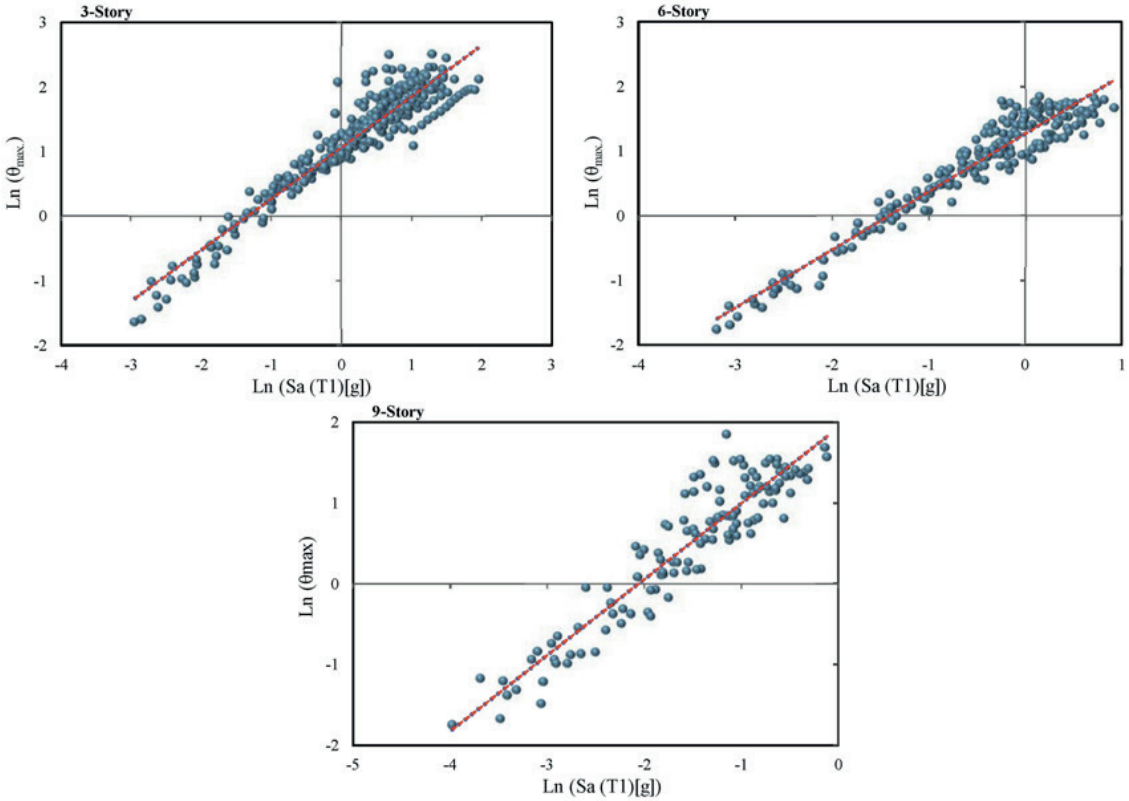

Fig. 11 Variation of logarithmic form of the θmax versus Sa (T1) [g].

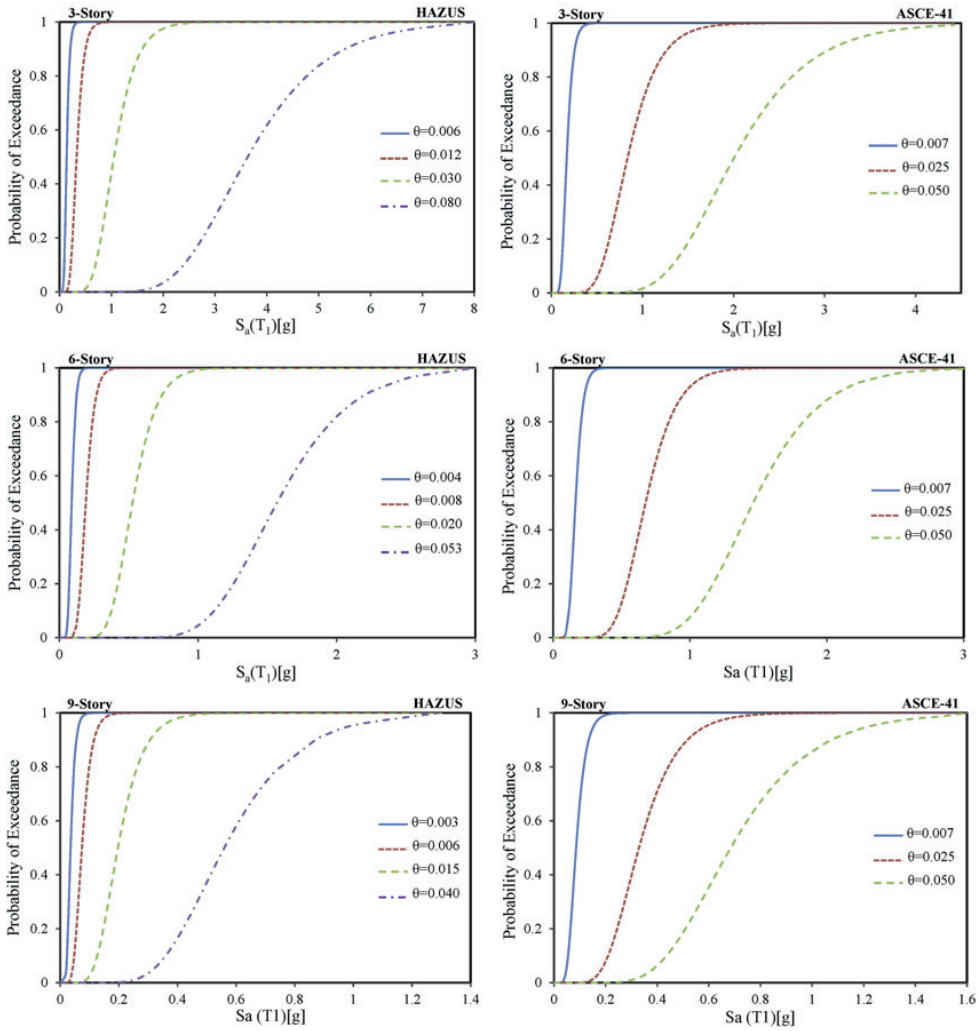

Fig. 12 Fragility curves of three, six, and nine-story in terms of the spectral acceleration.

8.2 Fragility and vulnerability curves

In this study, fragility curves are produced for three prototypes of CFT-MRF based on damage state levels specified in ASCE-41 [45] and HAZUS [52]. Furthermore, because of a lack of damage state levels for CFT-MRF structures in HAZUS and ASCE-41, the threshold of damage levels in steel MRF are selected. According to ASCE-41, the structural performance could be defined as three performance states: immediate occupancy (IO), where the building sustains very limited structural and nonstructural damages, and retains its pre-excitation capacity; life safety (LS), is defined as the performance level that building may suffer significant damage in structural and nonstructural components, but building preserves some margin against partial or complete collapse; and collapse prevention (CP), where major components of building experience significant damage and building has no safety against collapse. Above three performance states are defined by 0.7%, 2.5%, and 5% transient drifts, respectively. These three levels of damage could be assumed as corresponding to minor, moderate and severe damages. Four damage state of (1) slight, (2) moderate, (3) extensive, and (4) complete, are defined in HAZUS [52]. The damage levels proposed by HAZUS are presented in Table 4. Fig. 12 depicts the failure probability curves for three-, six- and nine-story RCFT-structures.

Table 4 Structural fragility curve parameters (HAZUS) [52]

Label	Type	Building code	Interstory drift at threshold of damage state			
			Slight	Moderate	Extensive	Complete
CFT-L	Low-rise	High	0.006	0.012	0.030	0.0800
CFT-M	Mid-rise	High	0.004	0.008	0.020	0.0533
CFT-H	High-rise	High	0.003	0.006	0.015	0.0400

The results denote that for a certain level of spectral acceleration the conditional probability tends to heighten as the height of building increases. The median (50% exceedance) of three-, six- and nine-story buildings based on damage state levels specified in ASCE-41 [45] are 0.167g, 0.164g, and 0.086g for the IO state ($\theta = 0.007$); 0.835g, 0.676g, and 0.329g for the LS state ($\theta = 0.025$); and 2.005g, 1.462g, and 0.685g for the CP state ($\theta = 0.05$), respectively.

Finally, vulnerability curves are developed for using in the seismic risk assessment of CFT-MRFs. Vulnerability curves are constructed based on the approach presented in HAZUS, using Eq.14. Fig.13 shows the vulnerability curve using slight, moderate, extensive and complete levels of damage for three-, six- and nine-story prototypes. These curves establish a direct relationship between ground motion intensities and the probability of exceeding losses. Results denote that the three-story building has the lowest probability of damage for a given level of ground motion intensity. The S_a correspond to damage ratio of three-, six- and nine-story buildings based on vulnerability curves specified in HAZUS [52] are 1.19g, 0.62g, and 0.2g for the 25% damage ratio; 2.33g, 1.05g, and 0.34g for the 50% damage ratio; and 3.54g, 1.55g, and 0.55g for the 75% damage ratio, respectively. Also, the outcomes of such assessments are crucial in the mitigation of huge losses subjected to future excitations.

9 Reliability analysis

To assess seismic risk to a structure, the annual probability of building that the drift demand exceeds certain value of damage can be represented by the form,

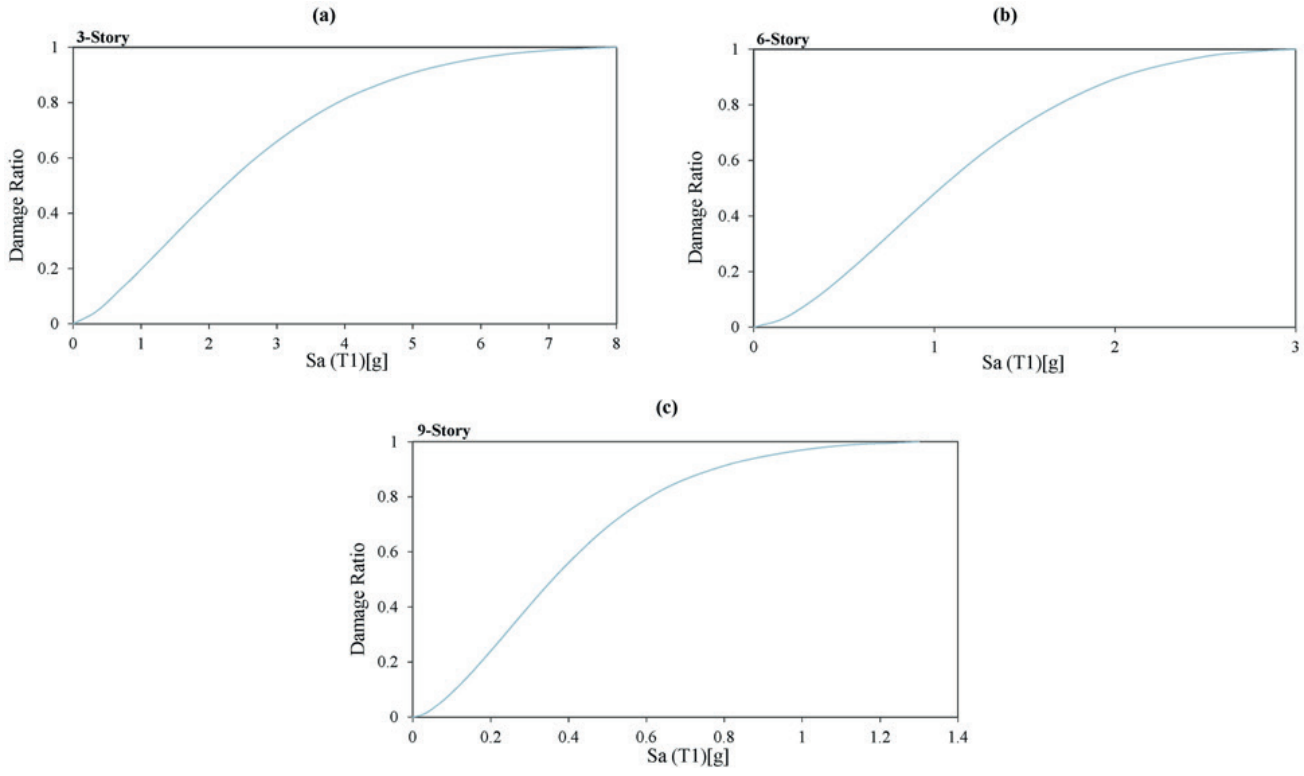

Fig. 13 Vulnerability curves of three prototype buildings: (a) three-story, (b) six-story, and (c) nine-story.

$$H_D(C) = P[C \le D] = \int P(D \ge C \mid S_a = x) \left| dH(x) \right| \quad (15)$$

Where, $P(D \ge C|S_a = x)$ is seismic fragility function, and H(x) defines mean annual frequency (MAF) that can be obtained from a seismic hazard analysis. The Eq. 16 was proposed by Cornell et al. [54] utilizes to calculate H(x).

$$H(S_a) = P[S_a \ge s_a] = k_0 s_a^{-k} \quad (16)$$

Where, k_0 and k are coefficients that can be calculated from log-log plot of standard hazard curve.

Using Eqs. 12 and 16, Eq. 15 can be modified as,

$$H_D(C) = P[C \le D] = H(s_a^c) \exp\left[\frac{k^2}{2b^2} \beta_{D|IM^2}\right] \quad (17)$$

$$s_a^c = \left(\frac{C}{a}\right)^{\frac{1}{b}} \quad (18)$$

Using spectral accelerations (5% damping) correspond to 2, 5, 10% probability of exceedance in 50 years were provided by USGS, the $S_a(T_1)$ at 2, 5, 10% are 0.78g, 0.54g, and 0.39g for the three-story building; 0.58g, 0.41g, and 0.29g for the six-story building; and 0.40g, 0.28g, and 0.2g for the nine-story building, respectively. Furthermore, for the three-story building, the constant parameters are k=2.3513 and k_0=2.36E-4; for the six-story building, k=2.2546 and k_0=1.42E-4; and for the nine-story building, k=2.2623 and k_0=6.52E-5. The annual probability of exceeding damage states (Eq. 15) is depicted in Fig. 14 for the three studied buildings.

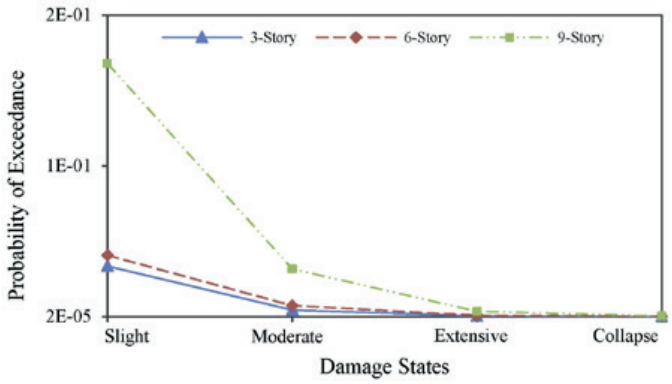

Fig. 14 Annual probability of exceedance for three prototype buildings.

10 Conclusions

This study performed the seismic failure probability and vulnerability assessment for three prototypes of steel-concrete composite structures using incremental dynamic analysis. Fragility curves are an appropriate tool for representing the seismic failure probabilities, and vulnerability curves relate uncertain loss to a measure of seismic excitation. The details of components modeling of RCFT-frame (RCFT column, steel beam, panel zone, and connection) in OpenSEES are explained, and the validation of proposed procedure is studied through comparisons with available experimental results. In order to carry out NTHA, a suite of 22 recorded ground motions were obtained from ground motion databases. Fragility curves were generated for three-, six- and nine-story CFT-MRFs based on damage state levels specified in ASCE-41 and HAZUS. The ground motion intensity and demand parameters were measured using the spectral acceleration at the first mode period of the building and maximum interstory drift ratio, respectively. The median of three-, six- and nine-story buildings based on damage levels specified in ASCE-41 are 0.167g, 0.164g, and 0.086g for the IO state; 0.835g, 0.676g, and 0.329g for the LS state; and 2.005g, 1.462g, and 0.685g for the CP state, respectively. The results demonstrate that, for a given spectral acceleration, the conditional probability tends to heighten as the height of building enhances. In order to convert fragility curves to vulnerability function, cumulative probabilities were differentiated to acquire discrete probability of each damage state. The vulnerability curves are developed and reliability analysis is performed for using in the seismic risk assessment of CFT-MRF structures. The correspond to damage ratio of three-, six- and nine-story prototype buildings are 1.19g, 0.62g, and 0.2g for the 25% damage ratio; 2.33g, 1.05g, and 0.34g for the 50% damage ratio; and 3.54g, 1.55g, and 0.55g for the 75% damage ratio, respectively. The reliability analysis shown that the nine-story building is highly sensitive to seismic excitation intensity.

References

[1] Schnabl, S., Jelenić, G., Planinc, I. „Analytical buckling of slender circular concrete-filled steel tubular columns with compliant interfaces". *Journal of Constructional Steel Research*, *115*, pp. 252–262. 2015. https://doi.org/10.1016/j.jcsr.2015.08.035

[2] Lee, C.-H., Kang, T. H.-K., Kim, S.-Y., Kang, K. „Strain compatibility method for the design of short rectangular concrete-filled tube columns under eccentric axial loads". *Construction and Building Materials*, *121*, pp. 143–153. 2016. https://doi.org/10.1016/j.conbuildmat.2016.05.145

[3] Duarte, A. P. C., Silva, B. A., Silvestre, N., de Brito, J., Júlio, E., Castro, J. M. „Tests and design of short steel tubes filled with rubberised concrete". *Engineering Structures*, *112*, pp. 274–286. 2016. https://doi.org/10.1016/j.engstruct.2016.01.018

[4] Lai, M. H., Ho, J. C. M. „A theoretical axial stress-strain model for circular concrete-filled-steel-tube columns". *Engineering Structures*, *125*, pp. 124–143. 2016. https://doi.org/10.1016/j.engstruct.2016.06.048

[5] Kawaguchi, J., Morino, S., Sugimoto, T., Shirai, J. „Experimental study on structural characteristics of portal frames consisting if square CFT columns". In: *Composite Construction in Steel and Concrete IV*. Banff, Canada. 2002. https://doi.org/10.1061/40616(281)63

[6] Herrera, R. A., Ricles, J. M., Sause, R. „Seismic Performance Evaluation of a Large-Scale Composite MRF Using Pseudodynamic Testing". *Journal of Structural Engineering*, *134*(2), pp. 279–288. 2008. https://doi.org/10.1061/(ASCE)0733-9445(2008)134:2(279)

[7] Tort, C., Hajjar, J. F. „Mixed finite-element modeling of rectangular concrete-filled steel tube members and frames under static and dynamic loads". *Journal of structural engineering*, *136*(6), pp. 654–664. 2009. https://doi.org/10.1061/(ASCE)ST.1943-541X.0000158

[8] Denavit, M. D., Hajjar, J. F. *Characterization of behavior of steel-concrete composite members and frames with applications for design*. Newmark Structural Engineering Laboratory. University of Illinois at Urbana-Champaign. 2014.

[9] Denavit, M. D., Hajjar, J. F. „Nonlinear Seismic Analysis of Circular Concrete-Filled Steel Tube Members and Frames". *Journal of Structural Engineering*, *138*(9), pp. 1089–1098. 2012. https://doi.org/10.1061/(ASCE)ST.1943-541X.0000544

[10] Skalomenos, K. A., Hatzigeorgiou, G. D., Beskos, D. E. „Modeling level selection for seismic analysis of concrete-filled steel tube/moment-resisting frames by using fragility curves". *Earthquake Engineering & Structural Dynamics*, *44*(2), pp. 199–220. 2015. https://doi.org/10.1002/eqe.2465

[11] Kamaris, G. S., Skalomenos, K. A., Hatzigeorgiou, G. D., Beskos, D. E. „Seismic damage estimation of in-plane regular steel/concrete composite moment resisting frames". *Engineering Structures*, *115*, pp. 67–77. 2016. https://doi.org/10.1016/j.engstruct.2016.01.053

[12] Denavit, M. D., Hajjar, J. F., Perea, T., Leon, R. T. „Stability Analysis and Design of Composite Structures". *Journal of Structural Engineering*, *142*(3), pp. 4015157. 2016. https://doi.org/10.1061/(ASCE)ST.1943-541X.0001434

[13] Sakino, K., Nakahara, H., Morino, S., Nishiyama, I. „Behavior of Centrally Loaded Concrete-Filled Steel-Tube Short Columns". *Journal of Structural Engineering*, *130*(2), pp. 180–188. 2004. https://doi.org/10.1061/(ASCE)0733-9445(2004)130:2(180)

[14] Varma, A. H., Ricles, J. M., Sause, R., Lu, L.-W. „Seismic Behavior and Design of High-Strength Square Concrete-Filled Steel Tube Beam Columns". *Journal of Structural Engineering*, *130*(2), pp. 169–179. 2004. https://doi.org/10.1061/(ASCE)0733-9445(2004)130:2(169)

[15] Tort, C., Hajjar, J. F. „Mixed Finite Element for Three-Dimensional Nonlinear Dynamic Analysis of Rectangular Concrete-Filled Steel Tube Beam-Columns". *Journal of Engineering Mechanics*, *136*(11), pp. 1329–1339. 2010. https://doi.org/10.1061/(ASCE)EM.1943-7889.0000179

[16] Perea, T., Leon, R. T., Hajjar, J. F., Denavit, M. D. „Full-Scale Tests of Slender Concrete-Filled Tubes: Axial Behavior". *Journal of Structural Engineering*, *139*(7), pp. 1249–1262. 2013. https://doi.org/10.1061/(ASCE)ST.1943-541X.0000784

[17] Perea, T., Leon, R. T., Hajjar, J. F., Denavit, M. D. „Full-Scale Tests of Slender Concrete-Filled Tubes: Interaction Behavior". Journal *of Structural Engineering*, *140*(9), pp. 4014054. 2014. https://doi.org/10.1061/(ASCE)ST.1943-541X.0000949

[18] Lai, Z., Varma, A. H., Griffis, L. G. „Analysis and Design of Noncompact and Slender CFT Beam-Columns". *Journal of Structural Engineering*, *142*(1), pp. 4015097. 2016. https://doi.org/10.1061/(ASCE)ST.1943-541X.0001349

[19] Skalomenos, K. A., Hatzigeorgiou, G. D., Beskos, D. E. „Parameter identification of three hysteretic models for the simulation of the response of CFT columns to cyclic loading". *Engineering Structures*, *61*, pp. 44–60. 2014. https://doi.org/10.1016/j.engstruct.2014.01.006

[20] Ahmadi, M., Naderpour, H., Kheyroddin, A. „Utilization of artificial neural networks to prediction of the capacity of CCFT short columns subject to short term axial load". *Archives of Civil and Mechanical Engineering*, *14*(3), pp. 510–517. 2014. https://doi.org/10.1016/j.acme.2014.01.006

[21] Ahmadi, M., Naderpour, H., Kheyroddin, A. „Performance of circular concrete filled steel tube members subjected to axial load". In *Fourth International Conference on Concrete & Development*. Tehran: Road , Housing and Development Research Center. 2013.

[22] Kheyroddin, A., Naderpour, H., Ahmadi, M. „Compressive strength of confined concrete in CCFST columns". *Journal of Rehabilitation in Civil Engineering*, *2*(1), pp. 106–113. 2014. https://doi.org/10.22075/jrce.2014.12

[23] Lai, Z., Varma, A. H. „Effective stress-strain relationships for analysis of noncompact and slender filled composite (CFT) members". *Engineering Structures*, *124*, pp. 457–472. 2016. https://doi.org/10.1016/j.engstruct.2016.06.028

[24] Xiang, X., Cai, C., Zhao, R., Peng, H. „Numerical analysis of recycled aggregate concrete-filled steel tube stub columns". *Advances in Structural Engineering*, *19*(5), pp. 717–729. 2016. https://doi.org/10.1177/1369433215618270

[25] Ricles, J. M., Peng, S. W., Lu, L. W. „Seismic Behavior of Composite Concrete Filled Steel Tube Column-Wide Flange Beam Moment Connections". *Journal of Structural Engineering*, *130*(2), pp. 223–232. 2004. https://doi.org/10.1061/(ASCE)0733-9445(2004)130:2(223)

[26] Wang, J., Zhang, L., Spencer, B. F. „Seismic response of extended end plate joints to concrete-filled steel tubular columns". *Engineering Structures*, *49*, pp. 876–892. 2013. https://doi.org/10.1016/j.engstruct.2013.01.001

[27] Ataei, A., Bradford, M. A., Valipour, H. R. „Experimental study of flush end plate beam-to-CFST column composite joints with deconstructable bolted shear connectors". *Engineering Structures*, *99*, pp. 616–630. 2015. https://doi.org/10.1016/j.engstruct.2015.05.012

[28] Kang, L., Leon, R. T., Lu, X. „A general analytical model for steel beam-to-CFT column connections in OpenSEES". *Journal of Constructional Steel Research*, *100*, pp. 82–96. 2014. https://doi.org/10.1016/j.jcsr.2014.04.022

[29] Frankie, T. M., Gencturk, B., Elnashai, A. S. „Simulation-Based Fragility Relationships for Unreinforced Masonry Buildings". *Journal of Structural Engineering*, *139*(3), pp. 400–410. 2013. https://doi.org/10.1061/(ASCE)ST.1943-541X.0000648

[30] Sadeghi, M., Ghafory-Ashtiany, M., Pakdel-Lahiji, N. „Developing seismic vulnerability curves for typical Iranian buildings". *Proceedings of the Institution of Mechanical Engineers, Part O: Journal of Risk and Reliability*, *229*(6), pp. 627–640. 2015. https://doi.org/10.1177/1748006X15596085

[31] Porter, K. *Beginner's guide to fragility, vulnerability, and risk*. University of Colorado Boulder. 2016.

[32] Ahmadi, M., Naderpour, H., Kheyroddin, A. „ANN Model for Predicting the Compressive Strength of Circular Steel-Confined Concrete". *International Journal of Civil Engineering*, *15*(2), pp. 213–221. 2017. https://doi.org/10.1007/s40999-016-0096-0

[33] Ahmadi, M. *Developing empirical approaches for determining the axial compressive capacity and compressive strength of confined concrete in circular concrete-filled steel tube columns (in Persian)*. Semnan University. 2012.

[34] McKenna, F., Fenves, G. L., Scott, M. H. „Open system for earthquake engineering simulation". *University of California, Berkeley, CA*. 2000. URL: http://opensees.berkeley.edu

[35] Chang, G. A., Mander, J. B. *Seismic energy based fatigue damage analysis of bridge columns: Part I-Evaluation of seismic capacity*. National Center for Earthquake Engineering Research Buffalo, NY. 1994.

[36] Tsai, W. T. „Uniaxial Compressional Stress-Strain Relation of Concrete". *Journal of Structural Engineering*, *114*(9), pp. 2133–2136. 1988. https://doi.org/10.1061/(ASCE)0733-9445(1988)114:9(2133)

[37] Shen, C., P. Mamaghani, I. H., Mizuno, E., Usami, T. „Cyclic Behavior of Structural Steels. II: Theory". *Journal of Engineering Mechanics*, *121*(11), pp. 1165–1172. 1995. https://doi.org/10.1061/(ASCE)0733-9399(1995)121:11(1165)

[38] Ibarra, L. F., Medina, R. A., Krawinkler, H. „Hysteretic models that incorporate strength and stiffness deterioration". *Earthquake Engineering & Structural Dynamics*, *34*(12), pp. 1489–1511. 2005. https://doi.org/10.1002/eqe.495

[39] Lignos, D. G., Krawinkler, H. „Deterioration Modeling of Steel Components in Support of Collapse Prediction of Steel Moment Frames under Earthquake Loading". *Journal of Structural Engineering*, *137*(11), pp. 1291–1302. 2011. https://doi.org/10.1061/(ASCE)ST.1943-541X.0000376

[40] Muhummud, T. *Seismic behavior and design of composite SMRFs with concrete filled steel tubular columns and steel wide flange beams*. Lehigh University, Bethlehem, Pennsylvania. 2003.

[41] Krawinkler, H. „Shear in beam-column joints in seismic design of steel frames". *Engineering Journal*, *15*(3), pp. 82–91. 1978.

[42] Sheet, I. S., Gunasekaran, U., MacRae, G. A. „Experimental investigation of CFT column to steel beam connections under cyclic loading". *Journal of Constructional Steel Research*, *86*, pp. 167–182. 2013. https://doi.org/10.1016/j.jcsr.2013.03.021

[43] American Society of Civil Engineers. *Minimum design loads for buildings and other structures: second Printing (ASCE/SEI 7)*. 2010.

[44] American Institute of Steel Construction. *Specification for structural steel buildings (ANSI/AISC 360)*. 2010.

[45] American Society of Civil Engineers. *Seismic rehabilitation of existing buildings (ASCE/SEI 41)*. 2006.

[46] Federal Emergency Management Agency. *Quantification of building seismic performance factors (FEMA P695)*. Applied Technology Council. 2009.

[47] Pacific Earthquake Engineering Research (PEER) Center. „PEER ground motion database". 2015.

[48] US Geological Survey. „Center for engineering strong motion data (CESMD)". 2015.

[49] Vamvatsikos, D., Cornell, C. A. „Incremental dynamic analysis". *Earthquake Engineering & Structural Dynamics*, *31*(3), pp. 491–514. 2002. DOI: https://doi.org/10.1002/eqe.141

[50] Rajeev, P., Tesfamariam, S. „Seismic fragilities for reinforced concrete buildings with consideration of irregularities". *Structural Safety*, *39*, pp. 1–13. 2012. https://doi.org/10.1016/j.strusafe.2012.06.001

[51] Jeon, J.-S., Lowes, L. N., DesRoches, R., Brilakis, I. „Fragility curves for non-ductile reinforced concrete frames that exhibit different component response mechanisms". *Engineering Structures*, *85*, pp. 127–143. 2015. https://doi.org/10.1016/j.engstruct.2014.12.009

[52] Federal Emergency Management Agency. *Multi-hazard loss estimation methodology, earthquake model, HAZUS-MH MR4 technical manual*. 2003.

[53] Federal Emergency Management Agency. *Earthquake damage evaluation data for California (ATC 13)*. Applied Technology Council. 1985.

[54] Cornell, C. A., Jalayer, F., Hamburger, R. O., Foutch, D. A. „Probabilistic Basis for 2000 SAC Federal Emergency Management Agency Steel Moment Frame Guidelines". *Journal of Structural Engineering*, *128*(4), pp. 526–533. 2002. https://doi.org/10.1061/(ASCE)0733-9445(2002)128:4(526)